nature communications

Article

https://doi.org/10.1038/s41467-025-59904-x

Durable response to CAR T is associated with elevated activation and clonotypic expansion of the cytotoxic native T cell repertoire

Received: 18 July 2024

Accepted: 2 May 2025

Published online: 23 May 2025

Check for updates

Giulia Cheloni[1,2,3,8], Dimitra Karagkouni[2,3,4,5,8], Yered Pita-Juarez[2,3,4,5], Daniela Torres[1], Eleni Kanata[4], Jessica Liegel[1,2,3], Zachary Avigan[1], Isabella Saldarriaga[1,2,3], Georges Chedid[1,2,3], Kathrine Rallis[1,2,3], Brodie Miles[6], Gayatri Tiwari[6], Jenny Kim[6], Mike Mattie[6], Jacalyn Rosenblatt[1,2,3], Ioannis S. Vlachos[2,3,4,5,7,9] & David Avigan[1,2,3,9]

While Chimeric Antigen Receptor (CAR) T cell therapy may result in durable remissions in recurrent large B cell lymphoma, persistence is limited and the mechanisms underlying long-term response are not fully elucidated. Using longitudinal single-cell immunoprofiling, here we compare the immune landscape in durable remission versus early relapse patients following CD19 CAR T cell infusion in the NCT02348216 (ZUMA-1) trial. Four weeks post-infusion, both cohorts demonstrate low circulating CAR T cells. We observe that long-term remission is associated with elevated native cytotoxic and proinflammatory effector cells, and post-infusion clonotypic expansion of effector memory T cells. Conversely, early relapse is associated with impaired NK cell cytotoxicity and elevated immunoregulatory cells, potentially dampening native T cell activation. Thus, we suggest that durable remission to CAR T is associated with a distinct T cell signature and pattern of clonotypic expansion within the native T cell compartment post-therapy, consistent with their contribution to the maintenance of response.

Chimeric antigen receptor (CAR) T cell therapy has transformed outcomes for patients with relapsed/refractory large B cell lymphoma (LBCL), demonstrating overall response rates of 52–74%, with ~40% of patients achieving durable remission[1–5]. While therapeutic resistance may be associated with immune escape due to the emergence of CD19-negative tumor variants, disease relapse can occur despite persistence of the target antigen as a result of loss or dysfunction of the CAR T cell populations. Previous studies have demonstrated that the increased presence of naïve and stem cell memory T cells at the time of CAR T production is associated with improved response[6–9], while the presence of terminal effector or dysfunctional cells has been associated with blunted in vivo CAR T expansion and therapeutic resistance[2,10–20]. Whereas the degree of in vivo CAR T expansion and persistence may be associated with disease response, maintenance of remission does not fully correlate with the kinetics of the CAR T population and may be observed despite the rapid clearance of CAR T cells, especially in

[1]Department of Medicine, Beth Israel Deaconess Medical Center, Boston, MA, USA. [2]Cancer Center, Beth Israel Deaconess Medical Center, Boston, MA, USA. [3]Harvard Medical School, Boston, MA, USA. [4]Department of Pathology, Beth Israel Deaconess Medical Center, Boston, MA, USA. [5]Broad Institute of MIT and Harvard, Cambridge, MA, USA. [6]Kite, a Gilead Company, Santa Monica, CA, USA. [7]Spatial Technologies Unit, Harvard Medical School Initiative for RNA Medicine, Boston, MA, USA. [8]These authors contributed equally: Giulia Cheloni, Dimitra Karagkouni. [9]These authors jointly supervised this work: Ioannis S. Vlachos, David Avigan. e-mail: davigan@bidmc.harvard.edu

CD28-based CAR constructs[2,11–15,17,18,21–23]. The impact of the native T cell repertoire in determining the durability of response has not been fully elucidated.

We postulated that the long-term efficacy of CAR T therapy is dependent on the downstream activation of non-CAR T cell populations and the development of an adaptive T cell response necessary to prevent disease recurrence. We hypothesized that CAR T-induced cytokine release and tumor lysis in an inflammatory context could facilitate the activation and clonotypic expansion of the native T cell repertoire, contributing to the maintenance of long-term response.

Using single-cell immunoprofiling, we perform a comparative analysis of the native T cell repertoire post-CAR T therapy in LBCL patients enrolled in the registrational trial of axicabtagene ciloleucel (Axi-cel) (ZUMA-1/NCT02348216) who achieved a durable response lasting greater than 1 year as compared to disease relapse within 6 months (Fig. 1A, B). Durable remission is associated with increased presence of distinct native T cell subsets characterized by elevated cytotoxicity, pro-inflammatory activity, or proliferative capacity. Single-cell T cell receptor (TCR) profiling reveals the emergence and expansion of dominant clonotypes within the non-CAR T cell populations post-CAR T infusion in patients demonstrating long-term response. Remarkably, the pattern of clonotypic expansion within the native T cell repertoire is highly predictive of subsequent clinical outcomes. While the targets of the T cell response have not been elucidated, negative TCR screening results against extensive libraries of common viral antigens are consistent with the emergence of tumor-specific immunity as a potential mediator of ongoing remission following CAR T therapy. Of note, early relapse is associated with increased presence of immunoregulatory cells that potentially blunt activation and expansion of the native T cell repertoire. These findings suggest that activation and clonotypic expansion of the native T cell repertoire contribute to the maintenance of disease remission following CAR T therapy for lymphoma.

Results

Study population and immune landscape annotation

PBMCs were obtained from 32 patients who underwent CD19-directed CAR T cell therapy in the registrational trial of axicabtagene ciloleucel (Axi-cel) (ZUMA-1/NCT02348216)[2,3] (Supplementary Data 1, Fig. 1A, B, and Supplementary Fig. 1A). Twenty-nine patients consented to provide clinical outcome data for the analysis and were segregated into three cohorts: (i) ongoing response lasting greater than 1 year (long-term responders, LtR, $n = 13$), (ii) disease relapse within 6 months after CAR T infusion (relapsed, R, $n = 8$), and (iii) stable or progressive disease at 1 month after CAR T infusion (non-responders, NR, $n = 8$) (Supplementary Data 1). Of note, no statistically significant differences were observed in the tumor burden at baseline between the different disease cohorts (Supplementary Data 1, LtR vs R, p value = 0.086, LtR vs NR, p value = 0.65, Student's t-test). Single-cell immunoprofiling was performed on PBMCs obtained at the time of cell collection for CAR T cell production (leukapheresis) and at 4 weeks, 6 months, and 12 months post-CAR T infusion. A total of 405,775 cells were captured post-quality control (QC) and partitioned into nine major lineages (Fig. 1C–E). A detailed cell population dictionary is provided in the Supplementary Notes.

Durable response is associated with elevated cytotoxicity of the non-CAR CD8 T cell compartment

Consistent with prior reports[23–29], CAR T cells represented only a small subset of the circulating T cells at 4 weeks after CAR T infusion, with clearance observed by 6 months (Fig. 2A). We did not detect significant differences in the CAR T cell proportions between the distinct patient cohorts (Fig. 2A). Gene profiling of CAR T cytotoxicity at 4 weeks in the LtR patients compared to R patients did not meet statistical significance, while the small number of cells per group (LTR: $n = 33$, R: $n = 11$, NR: $n = 84$) does not provide adequate power for the detection of subtle differences (LtR vs R, p value = 0.42; LtR vs NR; p value = 0.9, Wilcoxon rank-sum test, two-sided, Supplementary Fig. 1B).

Single-cell immunoprofiling of the native T cell compartment revealed a higher baseline abundance of T cells in LtR patients compared to both R and NR patients (Supplementary Fig. 1C and Supplementary Table 1). LtR patients exhibited significantly higher CD8 T cell abundance than R patients (Fig. 2B, Supplementary Fig. 1D, and Supplementary Table 2). Additionally, LtR patients were characterized by an overall higher T cell cytotoxicity, as captured by the expression of eight key marker genes *(GZMA, GZMB, GZMH, GZMM, GZMK, PRF1, GNLY,* and *NKG7*) compared to both R and NR patients at baseline, with more pronounced differences observed at 4 weeks post-infusion (Fig. 2C). Consistent with the higher cytotoxic gene signature, durable response was associated with the upregulation of multiple pro-inflammatory cytokines, including *IFNG*, *IL21*, *IL12*, *IL2*, *IL17A*, and *IL22*[30] at 4 weeks post-CAR T (Fig. 2D). In contrast, NR and R patients demonstrated upregulation of the inhibitory factors *TGFβ* and *IL6*, known to negatively regulate the antitumor activity of CD8 T cells[31]. T cells of R patients demonstrated upregulation of *JUN*-family genes (*JUN, JUNB, JUND*, Supplementary Fig. 1E), whose immunoregulatory effects include the induction of T-regulatory cell (Treg) effector programs[32], while both R and NR patients exhibited downregulation of key cytotoxic marker genes post-CAR T, such as *NKG7, GZMH*, and *GNLY* (Supplementary Fig. 1E).

Durable response is associated with elevated CD8 T effector memory cell subsets with cytotoxic and proliferative potential

To further interrogate the effector cell response in patients achieving durable remission, we characterized the relative frequency of non-CAR T cell subsets pre- and post-CAR T infusion. CD8 T cells were segregated into 14 subpopulations (Fig. 2E, F and Supplementary Notes), reflecting their identity within the pseudotime trajectory, ranging from naïve to terminally differentiated effector cells (Fig. 3A and Supplementary Fig. 2A). Consistent with prior studies, LtR demonstrated a higher proportion of naïve/central memory CD8 T cells at the time of leukapheresis[9,33,34] compared to R patients (Fig. 3A, B and Supplementary Table 3). In contrast, at 4 weeks post-CAR T infusion, lower proportions of naïve/central memory were observed in LtR compared to both baseline (LtR: Leukapheresis vs 4 weeks after CAR T; Leukapheresis vs 6 months after CAR T: P value = 0.006; 0.03, Wilcoxon signed-rank test, two-sided, Fig. 3C) and to R patients at the same timepoints (Fig. 3A, B and Supplementary Table 3). Durable response was also associated with higher frequency of distinct, more differentiated, and activated cytotoxic effector memory CD8 T (Tem) subsets compared to patients exhibiting early relapse (Fig. 3A, B, Supplementary Fig. 2B, and Supplementary Table 3). Among these cell subsets, TGFb1 + CXCR4+ early Tem were more abundant in the LtR post-CAR T infusion, compared to R patients (Fig. 3A, B and Supplementary Table 3). TGFb1 + CXCR4+ Tem displayed an intermediate state between memory precursor effector cells (MPEC) and highly activated cytotoxic effector cells[35–37] (Fig. 2F and Supplementary Fig. 2B). This population lacked classical markers of naïve/central memory T cells and highly expressed MPEC, cytotoxic, and memory markers including *CXCR4*, an essential factor for the homeostatic self-renewal of CD8 memory cells[38] (Fig. 2F). Additionally, TGFb1 + CXCR4+ Tem highly expressed *TGFb1* and *BCL3*, two factors that restrain T cell terminal differentiation consistent with an intermediate state between early memory T cells and highly activated cytotoxic effector cells[35–37] (Fig. 2F). LtR also exhibited elevated proportions of highly cytotoxic CD8 Tem cells pre-/post-CAR T, characterized by high expression of markers associated with enhanced antitumor immune response (*NKG7*, *IL32*[39,40]) or with circulating tumor-infiltrating lymphocytes (*KLRD1* and *CD74*[41]) (Figs. 2F, 3B and Supplementary Table 3). An additional Tem subset defined by upregulation of pro-inflammatory

https://doi.org/10.1038/s41467-025-59904-x

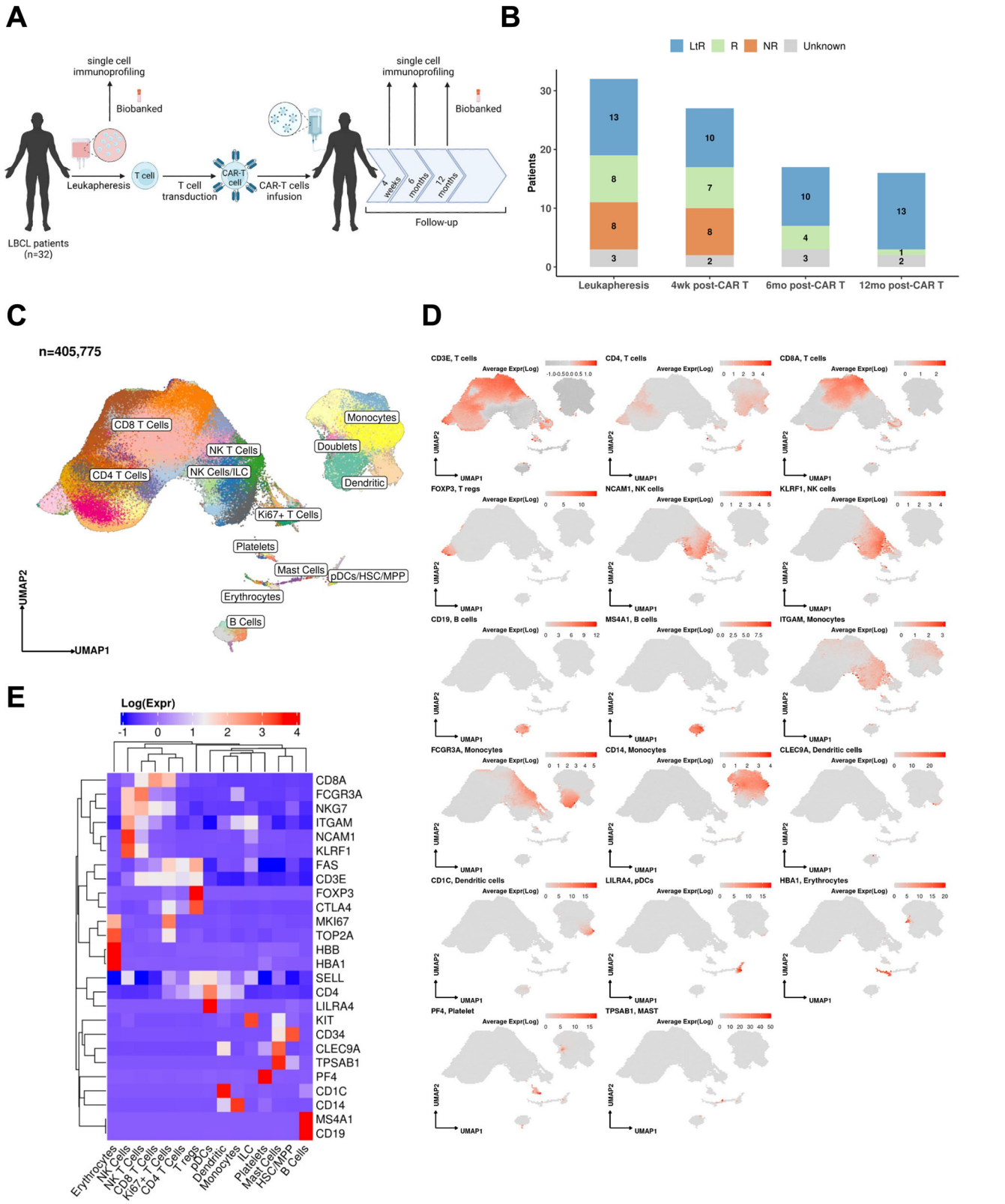

chemokines, cytokines and IFN-induced genes was more pronounced in LtR at baseline (CD8 Tem/Pro-inflammatory, Figs. 2F, 3B, Supplementary Fig. 2C, and Supplementary Table 3). Similar results were observed when comparing LtR and NR patients, with a higher proportion of highly cytotoxic CD8 Tem cells pre-/post-CAR T and of CD8 Tem/Pro-inflammatory cells 4 weeks post-CAR T being associated with durable response (Supplementary Fig. 2D and Supplementary Table 3).

Two additional Tem cell subsets (Ki67 + TOP2A+, Tex/Ki67 + IRF4+) were more abundant in the LtR at 4 weeks post-CAR T compared to baseline (LtR: Leukapheresis vs 4 weeks after CAR T, Ki67 + TOP2A+;Tex/Ki67 + IRF4+: P value = 0.024; 0.001, Wilcoxon signed-rank test, two-sided, Fig. 3C) as well as compared to R patients (Fig. 3B and Supplementary Table 3). These populations were characterized by co-expression of markers associated with T cell activation/exhaustion

Fig. 1 | The transcriptional states of the peripheral blood immune cells in CAR T-treated patients. A Sample processing pipeline depicting sample acquisition and preparation for scRNA-seq and scTCR-seq datasets. Created with BioRender.com; https://BioRender.com/p54q682. **B** Stacked barplots portraying the patient cohort ($n = 32$) and the distribution of patient samples collected for scRNA-seq and scTCR-seq. The number of patients with different clinical outcomes following CAR T infusion is portrayed (long-term responder-LtR, $n = 13$, Relapsed-R, $n = 8$, non-Responder-NR = 8, Unknown, $n = 3$). **C** Two-dimensional uniform manifold approximation and projection (UMAP) of all cells pre-/post-CAR T infusion. A total of 405,775 cells passed QC, capturing 73 populations, depicted with distinct colors, corresponding to nine major lineages: T cells (k = 264,059, 65% of all cells), B cells (k = 8255, 2% of all cells), natural killer (NK) and innate lymphoid (ILC) cells (k = 46,955, 11.6% of all cells), monocytes (k = 66,480, 16.4% of all cells), dendritic cells (DC, k = 6,228, 1.5% of all cells), plasmacytoid DC (pDC), and hematopoietic stem cells/multipotent progenitors (HSC/MPP) (k = 1,641, 0.4% of all cells), mast cells (k = 305, 0.075% of all cells), erythrocytes (k = 700, 0.17% of all cells), and platelets (k = 475, 0.12% of all cells). **D** Hexbin uniform manifold approximation and projection (UMAP) plots depicting the average gene expression for each major lineage marker in hexagons of 100 cells each. **E** Heatmap capturing the expression of marker genes across the major lineages.

and cell proliferation consistent with the early stage of dysfunction, previously described in a fraction of melanoma-infiltrating T cells[42] (Fig. 2F).

Durable response is associated with elevated CD4 cytotoxic T cells and diminished regulatory T cells

Non-CAR CD4 T cells were segregated into 14 subpopulations (Figs. 2F, 3B–D, Supplementary Fig. 3A–C, and Supplementary Notes). Similar to the pattern observed in the CD8 compartment, LtR demonstrated significantly increased proportions of CD4 cytotoxic T lymphocytes (CTL), characterized by high expression of cytotoxic markers (*GZMA, GZMB, GZMK, GZMH*, *GNLY*, Fig. 2F), compared to R patients across all timepoints (Fig. 3B, D and Supplementary Table 3). Of note, CD4 CTL increased in the post-CAR T period, with statistically significant higher proportion noted at 4 weeks post-CAR T infusion compared to baseline in LtR (LtR: Leukapheresis vs 4 weeks after CAR T, P value = 0.001, Wilcoxon signed-rank test, two-sided, Fig. 3C). In contrast, T regs were more abundant in the R patients, increasing from the time of leukapheresis to early post-CAR T infusion (Fig. 3B, D and Supplementary Table 3, Relapsed: Leukapheresis vs 4 weeks after CAR T, P value = 0.031, Wilcoxon signed-rank test, two-sided). Across all timepoints, R patients also presented higher proportions of other CD4 cell populations, including naïve (CD4 Tcm/naïve), naïve-like (CD4 Teh/TCF7 + LEF1+) and effector helper CD4 T cells (CD4 Th2, CD4 Th2/Th17, and CD4/Th17) (Figs. 2F, 3D, Supplementary Fig. 3A, and Supplementary Table 3).

The differences in the CD4 compartment between NR and LtR were less pronounced (Supplementary Fig. 3B, C and Supplementary Table 3). Nevertheless, significantly higher abundances of different CD4 subsets were observed in patients with refractory disease as compared to LtR at 4 weeks post-CAR T, including CD4 Tcm/naïve, CD4 Th2/Th17, CD4 Tem/Teh, and CD4 Tex/Ki67+ cell subsets (Supplementary Fig. 3C and Supplementary Table 3).

Early relapse is associated with impaired NK cell cytotoxic and chemotactic function post-CAR T infusion

NK cells exhibited significant upregulation of key cytotoxic and chemotactic genes (*GNLY, XCL2, IFIT2, CD52*, Supplementary Fig. 4A) at baseline in LtR compared to R. The higher cytotoxic and pro-inflammatory nature of the NK compartment in LtR compared to R became more pronounced 4 weeks post-CAR T therapy with upregulation of genes indicating cell activation, cytotoxicity, and a pro-inflammatory phenotype (*DUSP2, CCL5, IL32, GZMA, IFNG, PRF1, CCL3, CCL4, GZMB, CD74*, Fig. 4A, B). In NR patients, downregulation of immune regulatory genes (*NFKBIA, NFKBIZ, CD52*), pro-inflammatory and IFN-induced genes (*CCL3, CCL5, IL32, TNF, IFITM2, IFIT2*) pre-CAR T (Supplementary Fig. 4A), and the suppression of cytotoxic markers and pro-inflammatory chemokines (*CCL5, CCL3, CCL4, TNF, IFNG, GNLY*) 4 weeks post-CAR T, suggests a less severe but still impaired NK cell response (Fig. 4A). Of note, a higher relative abundance of CD56-bright immature NK cells was observed pre- and 4 weeks post-CAR T in NR compared to LtR, suggesting that an immature NK cell phenotype may be associated with reduced cytotoxic capacity and poor response to CAR T cell therapy (Supplementary Fig. 4B–D, Supplementary Table 4, and Supplementary Notes).

Durable response is associated with decreased Monocyte proportions

A higher abundance of monocytes was observed at baseline in R and NR patients compared to LtR (Supplementary Fig. 1B and Supplementary Table 1). In LtR patients, monocytes underwent a transition from a pro-inflammatory state at leukapheresis to an adaptive immunity-supporting phenotype by 4 weeks post-CAR T (Fig. 4C and Supplementary Fig. 4e). At leukapheresis, LtR monocytes exhibited heightened inflammatory activity driven by NF-κB and TLR signaling (*NFKBIA, CXCL8, CCL3*) and enhanced interferon pathways (*STAT1, IFI30*) (Supplementary Fig. 4E). This early immune priming likely facilitated effective T cell recruitment and antigen presentation[43]. By 4 weeks, LtR monocytes transitioned to a lower inflammatory state, with downregulation of NF-κB (*IL1B, NFKBIA*) and complement pathways (*C5AR1*) alongside upregulation of key antigen-presentation genes such as *CD86* and interferon pathways (*IFI30*) (Fig. 4C).

In R patients, this transition was incomplete. Monocytes retained stress and hypoxia-driven pathways (*HSPA5, SOD2*) alongside chronic inflammatory signaling via NF-κB (*NFKB1, TNFAIP3, ICAM1*) and oxidative stress genes (*MT-ND4L, MT-CYB*), indicative of a dysfunctional immune response[44–46] (Fig. 4C). NR patients exhibited persistent pro-inflammatory and complement pathway activation (*CXCL8, S100A9, C5AR1*) coupled with autophagy-related stress markers (*HMOX1, TIMP1, HSPA8*), maintaining a chronic inflammatory, exhaustion-prone microenvironment that likely impeded effective adaptive immunity[44,47–50] (Fig. 4C).

Monocytes were further segregated into seven subpopulations, differentiated by the expression of *CD14* and *FCGR3A/CD16* into classical, intermediate, and non-classical subsets[51], and further characterized based on their phagocytic phenotype or inflammatory profile (Supplementary Fig. 4F–H, Supplementary Notes). Post-CAR T, non-classical phagocytic monocytes, characterized by strong *FCGR3A/CD16*, low *CD14* expression, and elevated expression of interferon-induced and pro-inflammatory genes (*IFITM1, IFITM2, IFITM3, IL1B, TNF, CXCL16*, Supplementary Fig. 4F–H), were increased in R patients compared to LtR (Supplemental Fig. 4G and Supplementary Table 5), reflecting a dysregulated monocyte response that may contribute to unresolved inflammation and early relapse[52].

Ligand-receptor expression patterns revealed strong cell–cell interactions between monocytes and T cells, consistent with a potential immunoregulatory impact of these myeloid cells on the T cell populations (Fig. 4D, E). A CD86 signaling network via synapse formation with CTLA4 and CD28 on T cells was identified at 4 weeks post-CAR T infusion, representing dominant cellular interactions in the R patients between non-classical/phagocytic and pro-inflammatory monocyte subpopulations and T regulatory-like cells (Fig. 4D, E), suggesting a contributing role of monocytes in the T-regulatory immunosuppressive activity more prevalent in the relapsed patients following CAR T infusion.

https://doi.org/10.1038/s41467-025-59904-x

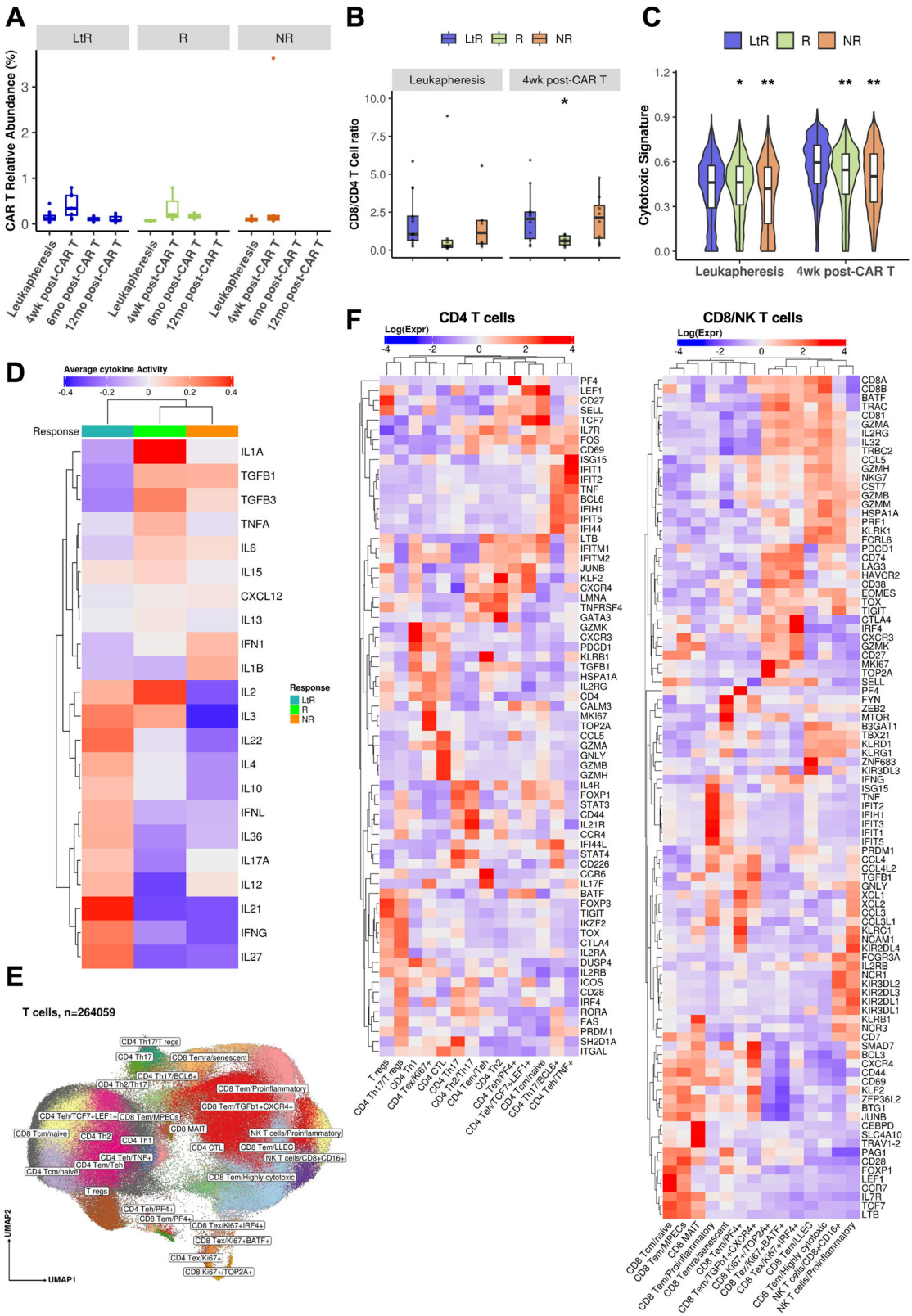

Durable response is associated with the emergence and expansion of dominant clonotypes within the effector cell repertoire post-CAR T infusion

We characterized the nature of clonotypic expansion in the non-CAR T lymphocyte compartment by leveraging single-cell immunoprofiling data capturing full-length paired α/β T cell receptors (TCR). 204,272 α/β TCR clonotypes were analyzed within the 28 non-CAR T cell populations (77.3% of all T cells), half of which represented unexpanded singletons (53.2%), based on the complementarity-determining region (CDR3, Supplementary Fig. 5A). Cytotoxic CD8 and CD4 T cells demonstrated greater clonal expansion compared to naive, CD4 effector helper, and CD8 naive-like T cells (Fig. 5A and Supplementary Fig. 5A). At 4 weeks post-CAR T, patients exhibiting durable response presented a statistically significant increase in the

Fig. 2 | Delineating the native immune repertoire associated with CAR T long-term efficacy. A CAR T relative abundance in the distinct patient groups (non-responders, NR, $n = 5$; relapsed, R, $n = 5$; long-term responders, LtR, $n = 13$) at the indicated timepoints is portrayed. Box plots show the median (line), interquartile range (IQR, box: 25th–75th percentiles), and whiskers (1.5 × IQR). Outliers are individual points. **B** Ratio of CD8 versus CD4 T cell proportions among the distinct clinical groups at baseline and 4 weeks post-CAR T infusion. Significantly different ratio between NR ($n = 8$) or R ($n = 7$) and LtR ($n = 13$) are denoted with * (P value <0.05; LtR vs R, p value = 0.086, LtR vs NR, p value = 0.65, Student's t-test, two-sided). Box plots show the median (line), IQR (box: 25th–75th percentiles), and whiskers (1.5 × IQR). Individual points represent each patient. **C** Ucell signature enrichment of CD8 T cells with the expression of cytotoxic genes *(GZMA, GZMB, GZMH, GZMK, GZMM, GNLY, NKG7, PRF1)*, among the distinct clinical groups at baseline and 4 weeks post-CAR T infusion. Significantly different expression profiles between NR ($n = 8$) or R ($n = 7$) and LtR ($n = 13$) are denoted with * (*FDR <0.05, **FDR <0.01; Leukapheresis: R vs LtR; NR vs LtR, FDR = 3.2×10^{-2}; 1.8×10^{-38}, 4 weeks after CAR T: R vs LtR; NR vs LtR, FDR = 1.4×10^{-93}; 8.37×10^{-181}, 6 months after CAR T: R vs LtR, FDR <2.2×10^{-16}, Wilcoxon rank-sum test, two-sided, Benjamini–Hochberg, FDR correction). Box plots show the median (line), IQR (box: 25th–75th percentiles), and whiskers (1.5 × IQR). **D** Average CytoSig cytokine signaling signatures across cells between the different cohorts 4 weeks post-CAR T infusion. Heatmap with blue-to-red gradient colors indicates the deviation from the overall mean. The different cohorts are portrayed with distinct colors. **E** Two-dimensional uniform manifold approximation and projection (UMAP) of T cells pre-/post-CAR T infusion. **F** Heatmaps capturing the expression of marker genes across the distinct (left) CD4 and (right) CD8 cell populations are displayed.

number of clonotypes with α/β TCR frequency >1 within the cytotoxic, proliferating, and pro-inflammatory CD8 and CD4 subsets (CD8 Tem/TGFb1 + CXCR4+, CD8 Tem/highly cytotoxic, CD8 Tem/pro-inflammatory, CD8 Ki67 + TOP2A+, CD8 Tex/Ki67 + IRF4+, and CD4 CTL, α/β TCR frequency >1, Fig. 5B and Supplementary Table 6) and shared α/β TCRs between the most expanded cytotoxic CD8 T cell populations (7–10% of the total CD8 T cells), denoting potential common antigenic targets among CD8 CTL populations (Supplementary Fig. 5B). We subsequently tracked the dynamics of clonotypes at 4 weeks post-CAR T compared to baseline. A high number of expanded clones was predominantly observed in LtR patients within the cytotoxic CD8 and CD4 subsets (CD8 Tem/TGFb1 + CXCR4+, CD8 Tem/highly cytotoxic, CD8 Tem/pro-inflammatory, CD4 CTL, Supplementary Fig. 6). Of note, 50% of LtR patients exhibited at least 2 expanded cytotoxic α/β TCRs at 4 weeks post-CAR T, based on increases in clonotype size relative to baseline, which was higher than the 16% observed in R patients and 12% in NR patients (Fig. 5C).

LtR patients demonstrated a progressive increase in the number of expanded cytotoxic clonotypes over time, at 6 months and 12 months post-CAR T infusion (Fig. 6A). By tracking the clonosize trajectory of individual 4-week-post-CAR T-expanded clonotypes, we observed that many peaked at 6 months and remained elevated at 12 months post-CAR T infusion (Fig. 6B and Supplementary Fig. 7A).

Only a small number of TCRs were identified to overlap with extensive compendia of CDR3 β TCRs recognizing viral antigens, including those derived from influenza, cytomegalovirus, and Epstein-Barr virus, while none of them presented significant expansion post-CAR T (Supplementary Fig. 7B).

We examined the potential association of T cell expansion dynamics at 4 weeks following CAR T infusion with therapeutic outcomes. In a multivariate Bayesian model, the pattern of clonotypic T cell expansion (α/β TCR frequency >1) at 4 weeks post-CAR T was highly predictive for segregating LtR from R patients ($n = 23$, AUC = 0.89, 95% CI:0.74–1, Fig. 6C). CAR T cell peak (Supplementary Data 1), which is a widely referenced predictive marker[22], demonstrated a lower predictive accuracy (AUC = 0.72, 95% CI:0.5–0.95, Fig. 6C and Supplementary Fig. 8). It is important to note that the present study does not comprise an independent validation cohort to assess the direct applicability of the model, and that CAR T cell peak has not been identified as a strong predictor in all published cohorts[53].

The T cell expansion (model output) and CAR T cell peak did not show a significant positive correlation ($r = 0.55$, $p = 0.12$, Pearson's correlation coefficient). We combined these metrics with logistic regression to explore whether the predictive performance is improved. We found that T cell expansion had a marginally significant positive association with the outcome in the combined model ($p = 0.07$), while the CAR T cell peak did not contribute meaningfully ($p = 0.79$). The combined model achieved a higher AUC than the CAR T cell peak alone (combined model: AUC = 0.89, 95% CI: 0.74–1; CAR T Peak: AUC = 0.72, 95% CI: 0.5–0.95) and was comparable to the T cell expansion model alone (AUC = 0.89, 95% CI: 0.74–1).

Discussion

CD19-directed CAR T cell therapies have transformed outcomes for patients with relapsed/refractory LBCL, with nearly 40% of patients exhibiting durable disease remission[2,4,5]. Understanding the factors characterizing persistent clinical response, as compared to early relapse, is of paramount importance for patient stratification and for the incorporation of novel strategies to enhance therapeutic efficacy.

Previous studies have demonstrated that elevation of naive and stem cell memory T cells in the leukapheresis product is associated with improved in vivo CAR T expansion and depth of response[6–9]. However, a lack of correlation between the persistence of the CAR T population and durability of response has been noted in some studies[22]. In the NCT02348216 study, while circulating CAR T cells decline rapidly within a few weeks of administration[2], ~40% of patients maintain long-term remission, far outliving CAR T cell presence[10]. We postulated that the elevated activation of the native T cell immunity plays a significant role in determining the durability of response after CAR T infusion. We further hypothesized that a cascade effect induced by CAR T-mediated inflammation and tumor lysis could boost the T cell response mediated by non-CAR effector T cell populations and could broaden the immune response beyond the CAR target antigen. To investigate our hypothesis, we performed longitudinal single-cell immunoprofiling of the native T cell compartment in patients participating in the NCT02348216 trial, with a comparative analysis between patients maintaining long-term remission and those experiencing relapse within 6 months of CAR T infusion. We interrogated samples at serial timepoints pre- and post-CAR T with a specific focus on 4 weeks post-CAR T infusion. This approach allows for the examination of the T cell compartment prior to disease relapse in order to assess potential associations with immune cell populations, T cell dynamics, or other markers associated with subsequent outcomes.

Consistent with prior reports, we showed that CAR T cells were present at relatively low levels at 4 weeks following infusion and declined thereafter. The relative abundance of CAR T cells at 4 weeks post-infusion did not correlate with the durability of response. At the time of leukapheresis, patients with durable remission showed a higher proportion of naive T cells, which constitutes a better substrate for the generation of CAR T cells with greater capacity for in vivo expansion and persistence[9,33,34]. In contrast, naïve T cells were reduced in the post-CAR T period in patients achieving long-term response as compared to the pre-CAR T timepoint. In addition, patients achieving a durable response exhibited higher proportions of cytotoxic CD8 and CD4 non-CAR T cells with an overall elevated cytotoxic signature at baseline that further increased at 4 weeks post-CAR T infusion as compared to patients subsequently experiencing early relapse. Heightened cytotoxicity in LtR at baseline may translate to a functionally more potent CAR T product. However, the rapid clearance of these cells, the absence of statistically significant differences in CAR T cytotoxic signature between the response cohorts, and the significant increase in cytotoxicity in the non-CAR T cells at 4 weeks post infusion in LtR are suggestive of a potential role of the native T cell repertoire in mediating disease response over time.

https://doi.org/10.1038/s41467-025-59904-x

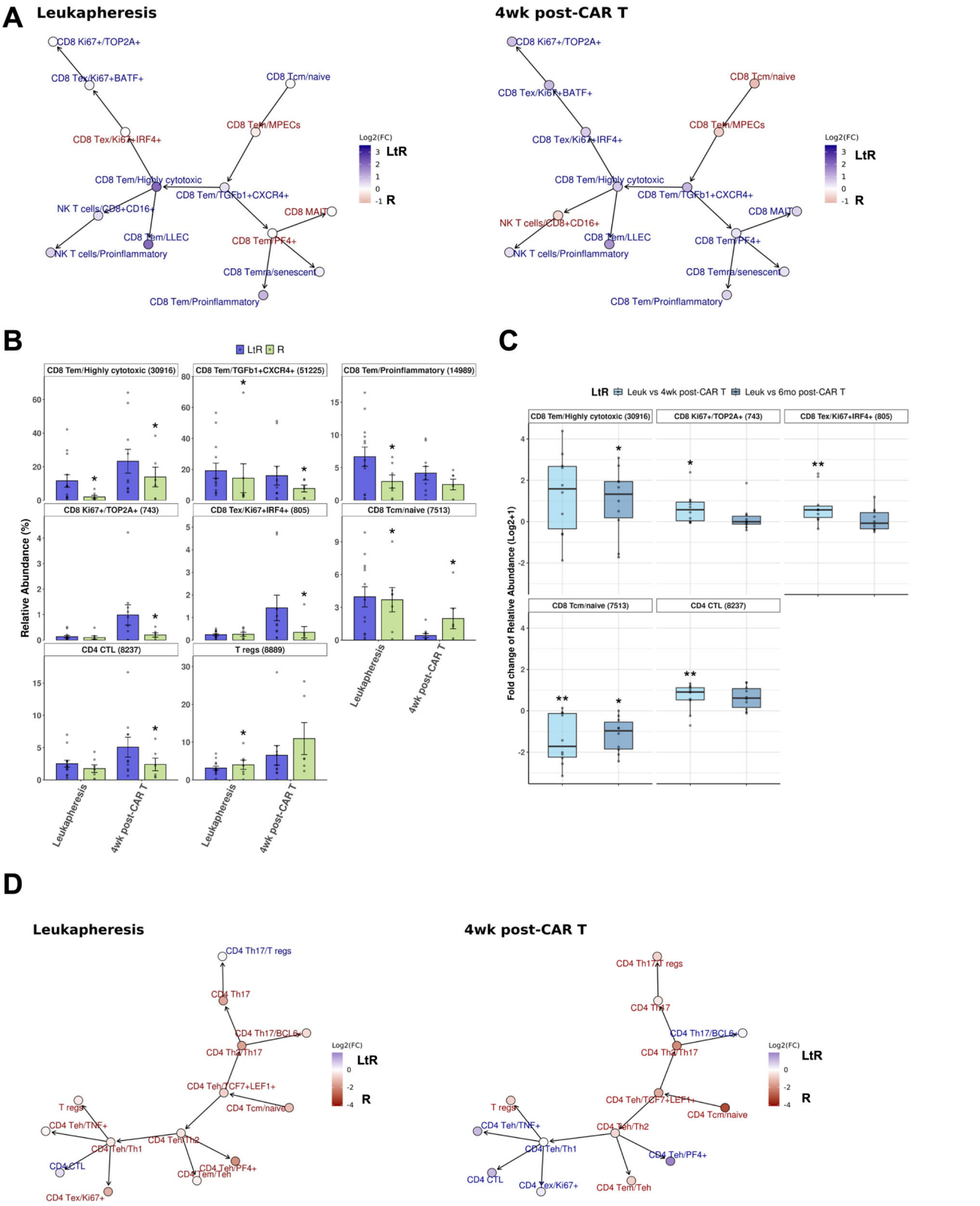

Accordingly, long-term responders demonstrated a unique T cell signature, as compared to patients experiencing early relapse, characterized by higher proportions of distinct activated non-CAR Tem subsets upregulating genes and cytokines associated with immune activation, inflammatory features, and cytotoxicity as well as subsets characterized by high proliferative potential, necessary for the maintenance of a memory response. These diverse cytotoxic Tem populations at different stages of activation/differentiation potentially act as a long-term barrier to tumor recurrence. In contrast, at 4 weeks post-CAR T therapy, patients with early relapse demonstrated a circulating T cell repertoire biased towards naïve and early memory cells with minimal cytotoxic capacity. The risk of subsequent relapse was also associated with higher proportions of native T regs, consistent with their immunosuppressive regulation

Fig. 3 | Charting the CD8/NK T and CD4 cell states associated with CAR T long-term efficacy. A Trajectory of CD8/NK T cell lineages, coupled with cell composition fold-change differences (log2 scale) between long-term responders (LtR, $n = 13$) and relapsed (R, $n = 7$) at baseline and 4 weeks post-CAR T infusion. **B** Cell proportion differences in CD8 and CD4 T cell states among the LtR ($n = 13$) and R patients ($n = 7$) at baseline and 4 weeks post-CAR T infusion. The relevant bars denote the mean ± standard deviation (SD) of the proportions for each patient group. The number of cells in each cell population is denoted in parenthesis. Significantly different proportions between R and LtR are denoted with * (*FDR <0.01; Binomial generalized linear model, Benjamini–Hochberg, FDR correction). **C** Fold-change differences (log_2 scale) in per-patient proportions of CD8 and CD4 T cell states at baseline versus post-CAR T infusion timepoints in LtR ($n = 13$). Significant differences between post-CAR T timepoints and baseline are denoted with * (*FDR <0.05, **FDR <0.01, Wilcoxon signed-rank test, two-sided, Benjamini–Hochberg, FDR correction). Box plots show the median (line), interquartile range (IQR, box: 25th–75th percentiles), and whiskers (1.5 × IQR). Individual points represent each patient. **D** Trajectory of CD4 T cell lineages, coupled with cell composition fold-change differences (log2 scale) between LtR ($n = 13$) and R ($n = 6$) at baseline and 4 weeks post-CAR T infusion.

of the cytotoxic T cell compartment, as previously reported[54–57]. Of note, patients with disease refractory to CAR T therapy demonstrated differences in the immune milieu compared to those who experienced an initial response followed by early relapse. In the case of primary resistance, the tumor's intrinsic features may play a more significant role than the immune milieu in driving therapeutic failure.

As compared to R patients, LtR demonstrated an increase in the number of expanded clonotypes at baseline and at 4 weeks post-CAR T therapy within the critical cytotoxic and pro-inflammatory effector cell populations. Of note, 50% of LtR patients demonstrated multiple α/β TCRs undergoing expansion at 4 weeks post-CAR T compared to baseline, with this expansion further increasing at subsequent timepoints. Tracking the relative clonosize of several of these individual TCR sequences revealed that many peaked at 6 months post-CAR T infusion and remained elevated at 1 year.

The elevated levels of clonotypic expansion within the cytotoxic T cell populations observed in LtR patients may serve as important mediators of disease response. Clonal expansion of cytotoxic non-CAR T effector cell populations strongly correlated with durable response post-CAR T therapy. However, independent validation studies are required to assess its applicability as a means for patient stratification. Of note, there was no correlation between clonal T cell and peak of CAR T expansion. It is possible that at least part of the antigens recognized by these expanded T cell clones are tumor-specific antigens made available after CAR T-mediated tumor lysis. Notably, the dominant clonotypes did not demonstrate viral specificity based on a screen of common viral-reactive TCRs. However, the nature of the antigenic targets recognized by the dominant clonotypes identified in patients achieving durable remission has not been elucidated. It is possible that some of the dominant clones represent cytotoxic bystander T cells, activated by cytokines or the release of tumor antigens following tumor lysis, that may contribute to the antitumor effect in the absence of direct TCR-mediated cytotoxicity. Further investigation is required to match the T cell clonotypes with their cognate antigens. Importantly, even though the identified clonotypes were present in the periphery rather than in the tumor bed, recent reports have demonstrated that T cell clonal dynamics in the tumor are reflected in the periphery[58], further strengthening the significance of our findings.

The clonal expansion of the native cytotoxic T cell repertoire following CAR T-driven tumor lysis is likely dependent on the uptake and presentation of antigens by antigen-presenting cells (APC) and on the functional competency of the non-CAR T cell populations. Accordingly, we observed that impaired NK cell cytotoxicity and elevation in immunoregulatory cells, including inflammatory monocytes, is associated with early relapse and likely contribute to sustained chronic inflammation and immune exhaustion, ultimately dampening T cell activation[22,59]. The role of immunomodulatory therapy, such as checkpoint inhibitors, in helping to drive these responses could prove to be of paramount importance. Additionally, CAR constructs incorporating cytokines to recruit APCs have been proven to increase CAR T antitumor activity[60,61], while pre-clinical studies have demonstrated synergy between vaccine-mediated stimulation of native immunity and CAR T therapy[62].

In summary, these findings are consistent with our hypothesis that the state of the native T cell repertoire is predictive of clinical outcomes, differentiating patients with early disease relapse from those maintaining durable response after CAR T therapy (Fig. 7) and that CAR T cell treatment triggers a long-term sustained cytotoxic response within the endogenous non-CAR T cell repertoire that may contribute to long-term remission. Elucidation of the targets recognized by the dominant highly expanded TCRs across long-term responder patients is currently being explored and may provide targets for adoptive T cell or cancer vaccine therapy. Combination cell-based therapy to facilitate epitope spreading and the development of a sustained antitumor immunity could represent a new frontier in CAR T-based immunotherapy.

Methods

Patient cohort

Ninety-two peripheral blood mononuclear cell (PBMC) samples from 32 patients with relapsed/refractory LBCL, treated with Axi-cel in the NCT02348216 trial (ZUMA-1), were analyzed. The patients had previously received an anti-CD20 antibody-containing regimen and anthracycline-containing chemotherapy and demonstrated refractory or relapsed disease to the previous lines of therapy (Supplementary Data 1). Disease burden at baseline and response was determined using the Lugano criteria incorporating the sum of the products of the longest perpendicular diameters (SPD) (Supplementary Data 1). Lymphodepleting chemotherapy prior to CAR T infusion consisted of cyclophosphamide and fludarabine. Objective responses at 1 month from CAR T infusion were assessed using revised IWG response criteria for malignant lymphoma[63].

The study protocol for the single-arm, multicenter, registrational ZUMA-1 study of axi-cel in patients with relapsed LBCL was previously described[2,3]. Each study site's institutional review board reviewed and approved the study protocol and amendments, and all patients provided written informed consent. The study was done according to the International Conference on Harmonization Good Clinical Practice guidelines. Patients in the ZUMA-1 study did not receive compensation for their participation.

Single-cell RNA and TCR library preparation and sequencing

Single-cell immunoprofiling was performed on PBMC samples collected from 32 LBCL patients at leukapheresis and at 4 weeks, 6 months, and 12 months post-CAR T infusion. For each sample, 8000–10,000 cells were loaded in one channel of a Chromium Chip K (10x Genomics, PN-1000286) and profiled using the Chromium Next GEM Single Cell 5′ Kit v2 (10x Genomics, PN-1000263). Full-length paired α/β TCR libraries were obtained using the Chromium Single Cell V(D)J Enrichment Human T Cell (10x Genomics, PN-1000252). cDNA, gene expression libraries, and TCR libraries were assessed using the DNA High Sensitivity Bioanalyzer Chip (Agilent, 5067-4626). Gene expression or TCR libraries were pooled and sequenced on the NovaSeq (Illumina) using the following parameters: 20,000 or 50,000

https://doi.org/10.1038/s41467-025-59904-x

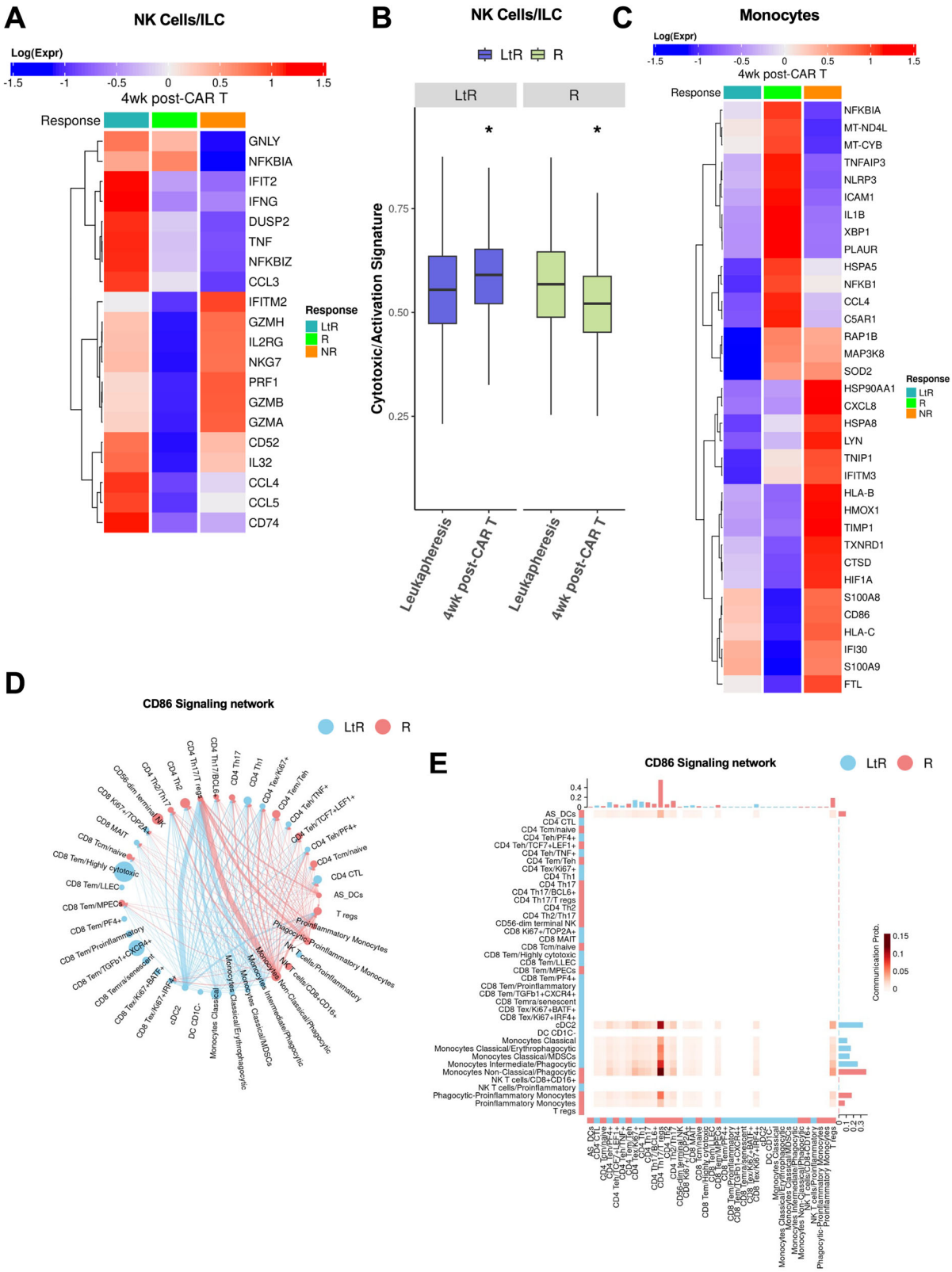

read pairs per cell for TCR or gene expression library, respectively; paired-end, dual indexing; read 1:26 cycles, i7 index:10 cycles, i5 index:10 cycles, Read 2:90 cycles.

scRNA sequencing preprocessing and sample integration

Cell assignment and gene expression quantification were applied with Cellranger v.4.0.0[64]. Empty droplets were removed using DropletUtils v.1.22.0[65,66] (FDR <0.05) and by evaluating specific quality metrics, including mitochondrial content (<10%), number of genes detected in each cell (1400 <n < 5500), and the total number of unique molecules detected within a cell (250 <n < 27,000). All samples were utilized for clustering and cell type identification. One patient with an insufficient yield of cells across all timepoints (P13, Relapsed, $n = 312$ cells, Supplementary Fig. 1A) was excluded from the downstream analysis and

https://doi.org/10.1038/s41467-025-59904-x

Fig. 4 | Charting the NK and Monocyte cell states associated with CAR T long-term efficacy. A Heatmap showing the average expression of differentially expressed genes in NK cells/ILC associated with activation and cytotoxic activity between long-term responders (LtR) and relapsed (R) or non-responders (NR) at 4 weeks post-CAR T infusion. Distinct colors represent the different cohorts, and gene expression profiles (log scale) are depicted using a blue-to-red gradient. **B** Ucell signature enrichment of NK cells/ILC with the expression of cytotoxic and activation genes (*CCL5, IL32, GNLY, GZMA, GZMH, CCL3, CCL4, NKG7, CD74, GZMB, PRF1, IL2RG, IFITM2, DUSP2, CD52, IFIT2, NFKBIA, CCL4, IFNG, TNF, NFKBIZ*), between baseline and 4 weeks post-CAR T infusion for the LtR ($n = 13$) and R ($n = 7$) patients. Significantly different expression profiles between timepoints are denoted with * (*FDR <0.01; Leukapheresis vs 4wk post-CAR T, LtR;R: FDR = 3.96×10^{-4}1;2.79×10^{-49}, Wilcoxon rank-sum test, two-sided, Benjamini–Hochberg, FDR correction). Box plots show the median (line), inter-quartile range (IQR, box: 25th–75th percentiles), and whiskers (1.5 × IQR). **C** Heatmap showing the average expression of differentially expressed genes in monocytes between LtR and R or NR 4 weeks post-CAR T infusion. Distinct colors represent the different cohorts, and gene expression profiles (log scale) are depicted using a blue-to-red gradient. **D** Chord diagram portraying the aggregated cell–cell communication in the CD86 signaling network. Thicker edge lines indicate stronger cell–cell interactions. Circle sizes are proportional to the number of cells in each cell population, while distinct colors are associated with the different cell types. Donor edge-line and circle color are portrayed in blue (increased in LtR) or red (increased in R), concordantly with the cell composition fold-change differences between LtR ($n = 10$) and R ($n = 4$) patients at 4 weeks post-CAR T infusion. **E** Heatmap of relative cell–cell communication probability in the CD86 signaling network among cell populations, shown in a white-to-red gradient (low to high). Barplots depict the total communication probability of each population with other cell types, colored blue (higher in LtR) or red (higher in R), reflecting fold-change differences at 4 weeks post-CAR T infusion.

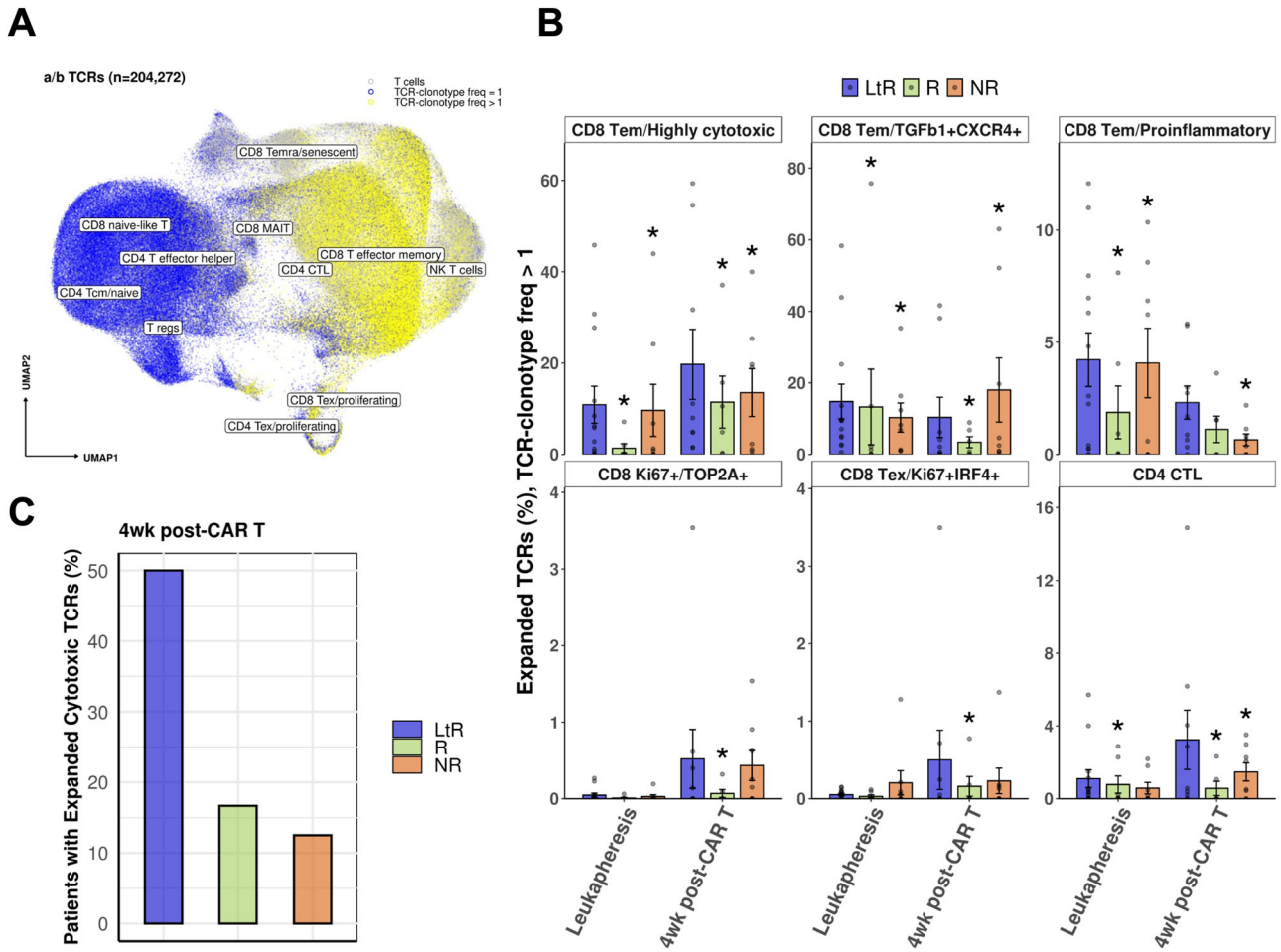

Fig. 5 | T Lymphocyte clonal expansion in CAR T-treated patients. A T cell receptor clonality at single-cell resolution is portrayed with distinct colors in two-dimensional uniform manifold approximation and projection (UMAP) of all T cells. T cells with TCR frequencies of 1 and more than 1 are marked with blue and yellow, respectively. T cells with no matching T cell receptors are marked in gray. **B** Barplots portraying the percentage of expanded paired α/β TCRs (frequency >1) in CD8 and CD4 cytotoxic, proliferating, and pro-inflammatory T cell states across distinct clinical groups at baseline and 4 weeks post-CAR T infusion. The relevant bars denote the mean ± standard deviation (SD) of the expanded TCRs relative to the total T cells in each patient group. Significant differences between non-responders (NR, $n = 8$) or relapsed patients (R, $n = 7$) and long-term responders (LtR, $n = 13$) are denoted with * (FDR <0.01; Binomial generalized linear model, Benjamini–Hochberg, FDR correction). **C** The percentages of patients with at least two expanded cytotoxic α/β CD8 T effector memory (Tem/highly cytotoxic, Tem/pro-inflammatory, Tem/TGFb1 + CXCR4+) and CD4 cytotoxic T lymphocyte (CD4 CTL) clonotypes, defined by significant increases in clonotype size relative to baseline, are shown for the different cohorts 4 weeks post-CAR T infusion.

the comparisons among clinical conditions. scRNA-seq samples were integrated into a single gene expression matrix and analyzed using Seurat v.3.2.3[67]. After normalization and log transformation, variable genes were defined with FindVariableFeatures from Seurat. Dimensionality reduction was applied on the first 30 PCA-retrieved principal components (PC) and the top 2000 variable genes. Samples were corrected for technical noise using each chip as a separate batch in Harmony v.0.1.0[68]. Cluster identification and Uniform Manifold Approximation and Projection (UMAP) embedding estimation were performed on the harmonized embeddings. Hexbin plots and hexagon

https://doi.org/10.1038/s41467-025-59904-x

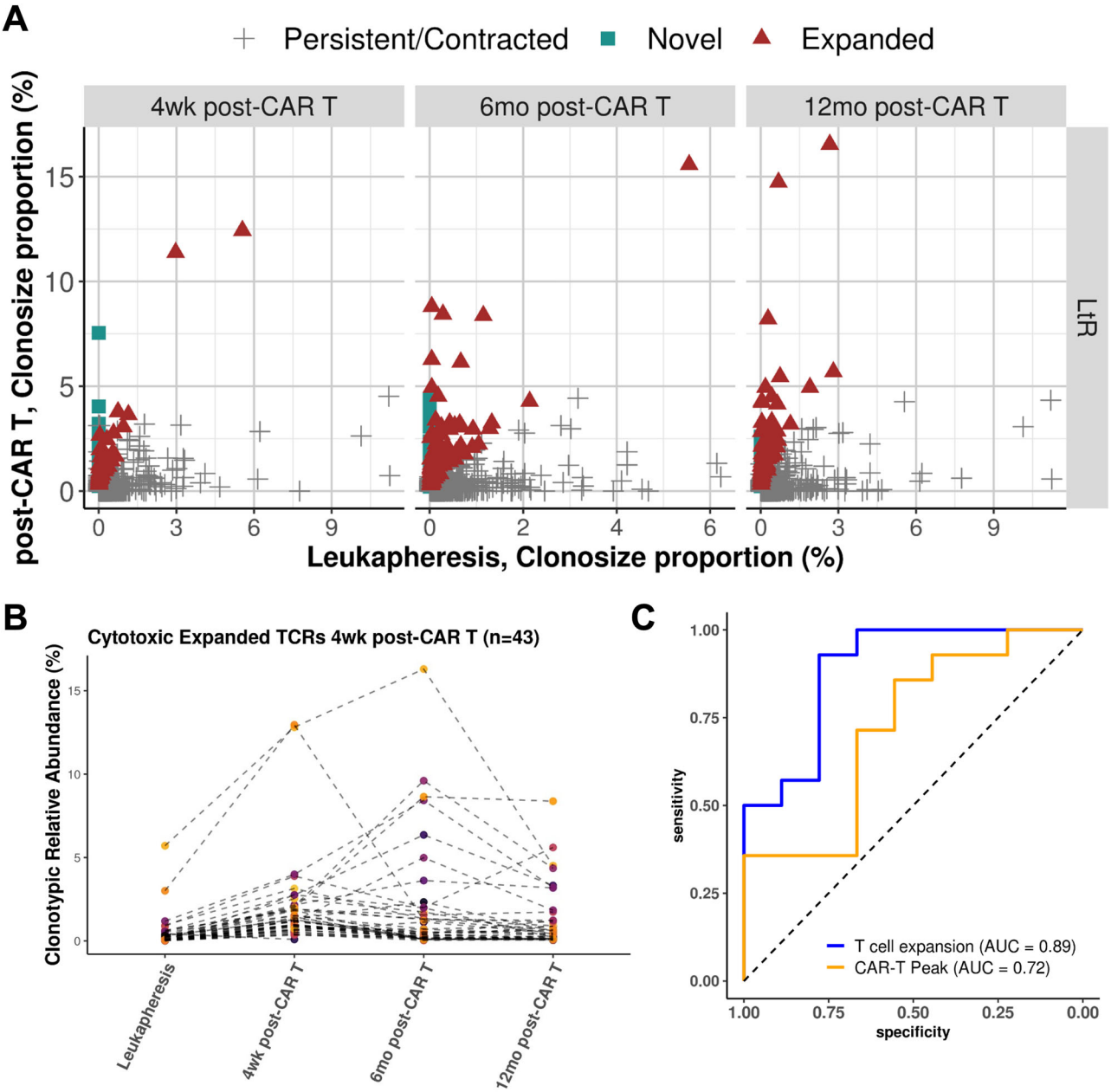

Fig. 6 | T Lymphocyte clonal expansion in CAR T-treated long-term responder (LtR) patients. A The α/β CD8 T effector memory (Tem/Highly cytotoxic, Tem/Pro-inflammatory, Tem/TGFb1+ CXCR4+) and CD4 CTL clonotype occurrence at baseline versus 4 weeks, 6 months, or 12 months post-CAR T for LtR patients. Clonosize-proportion changes among the pairwise timepoint comparisons of expanded (Fold-change >1, FDR <0.05, Fisher's exact test, Benjamini–Hochberg FDR correction), novel (Leukapheresis clonosize proportion = 0, FDR <0.05, Fisher's exact test, Benjamini–Hochberg FDR correction), and persistent/contracted clonotypes (persistent: FDR >0.05, Fisher's exact test, Benjamini–Hochberg FDR correction, and/or Fold-change = 1; contracted: Fold-change <1, FDR <0.05, Fisher's exact test, Benjamini–Hochberg FDR correction), are portrayed with red, cyan, and gray respectively. **B** Line plots depicting the clonosize-proportion changes of the expanded clonotypes at 4 weeks post-CAR T ($n = 43$) for each LtR patient shown in (**A**) across the time axis. **C** Receiver operating characteristic (ROC) curves showing the ability of the T cell expansion model and the CAR T peak classifications to distinguish between long-term responder patients and patients with relapsed/refractory disease 4 weeks post-CAR T. An area under the curve (AUC) score is portrayed for both models.

cells were defined by considering a neighborhood of 100 cells in each case and computed with the schex v.1.0.55 R package[69]. For CAR T cell identification, human and Axi-cel genomes were combined in the cell assignment process. Cells presenting footprints of CAR T expression (≥1 read counts on Axi-cel genome) are retained for further analysis.

Cell type identification

For the cell type identification, a two-step procedure was followed: (i) identification of major compartments, followed by (ii) iterative sub-clustering to define the specific cell populations. FindClusters function in Seurat v.3.2.3 was applied to the harmonized embeddings to define major compartments. For each major compartment, the top 2000 variable genes were utilized to re-harmonize the cells. The sub-clustering on the newly retrieved nearest neighbor graphs was accomplished with the FindClusters function. Cell type characterization was performed by using in-silico approaches, including SingleR v1.0.6[70] and CellTypist v.0.1.9[71], coupled with experts' manual annotation.

https://doi.org/10.1038/s41467-025-59904-x

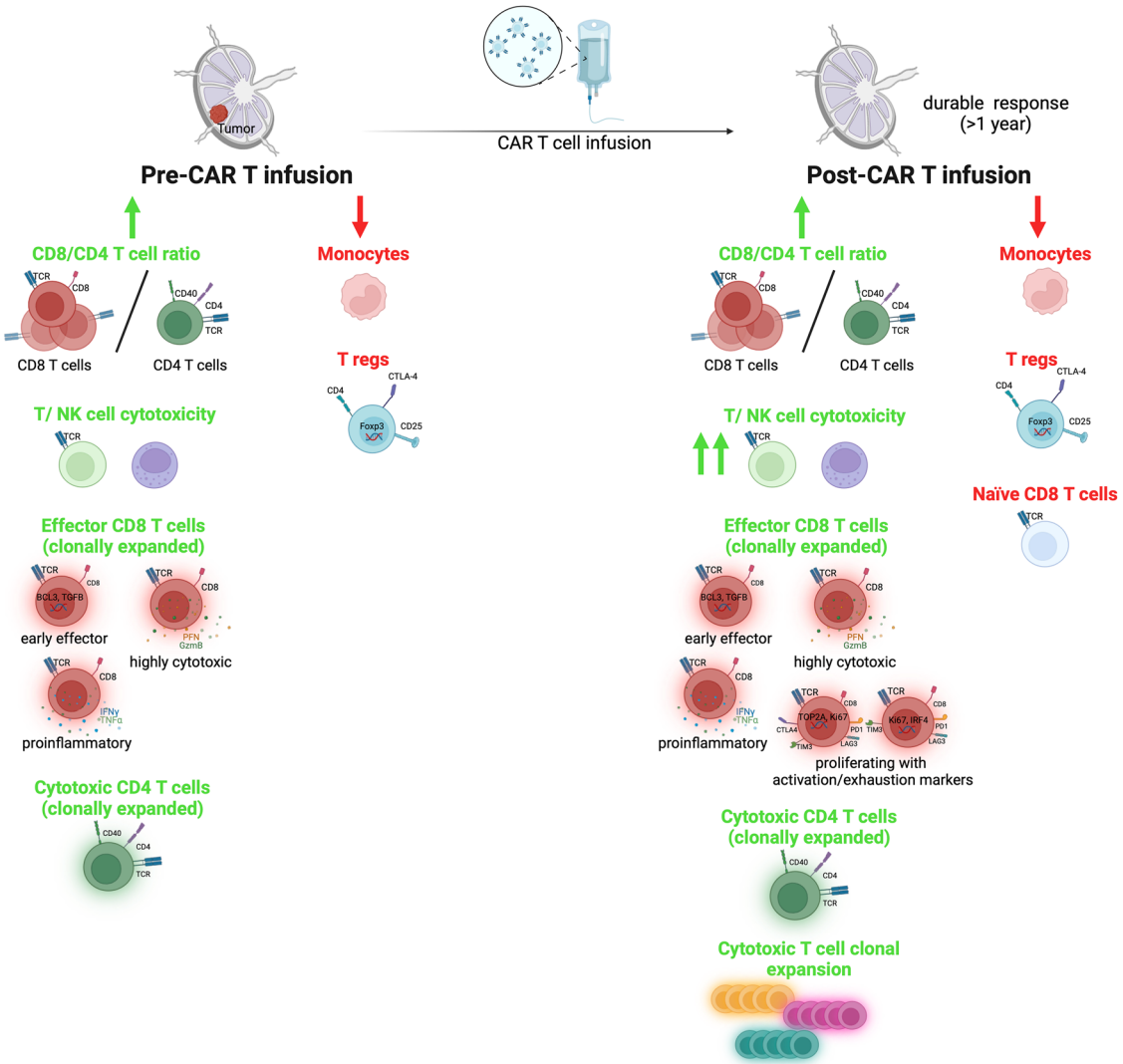

Fig. 7 | Long-term response to CAR T therapy is associated with a unique pre- and post-infusion peripheral blood immune landscape. Visual representation of key immune features associated with durable CAR T response. Created in BioRender. https://BioRender.com/y55l366.

Cell doublet detection

For cell doublet detection, three different approaches were utilized, Scrublet v.0.2.3[72], Pegasus v.0.1.3[73,74], and DoubletFinder v.2.0.2[75], per sample. Each method characterizes singlet or doublet cells. After sample integration and cluster identification, an enrichment test was applied to each cluster and method. Doublet-enriched clusters (FDR <0.05, Fisher's extract test), characterized by at least two methods, were marked as doublets accordingly. Nine clusters (k = 10,677) were defined as enriched in doublets and removed from the downstream analysis.

Cell-type gene marker detection

Cluster gene marker detection was performed by using limma-trend v.3.42.2[76,77]. Gene marker detection was performed at two levels: among (i) all the defined clusters and (ii) the clusters of the distinct lineages. Specifically, in each level of analysis, genes expressed in at least 10% of the cells of at least one cluster were retained, followed by TMM normalization[78] implemented in edgeR v.3.28.1[79]. A linear model using cluster and chip as covariates was fitted and modeled with the limma-trend method[76,77] and empirical Bayes procedure[80]. By using contrasts, significantly differentiated genes were retained per cluster (FDR <0.05, cluster coefficient >75% of all other clusters).

Differential gene expression analysis and cytokine signature scores across clinical groups

Differential gene expression analysis was conducted among the distinct clinical groups using the limma-trend[76,77]. Genes expressed on at least 10% of the cells of at least one sample were retained, followed by TMM normalization[78] implemented in edgeR v.3.28.1[79]. A linear model using clinical response and chip as covariates was fitted and modeled with the limma-trend method[76,77] and empirical Bayes procedure[80]. By using contrasts, significantly differentiated genes among the clinical groups at each timepoint were retained (FDR <0.05). Cytotoxicity gene and cytokine signature scores were calculated with UCell v.2.6.2 signature enrichment analysis[81] and CytoSig[82] per sample, respectively. CytoSig scores per cytokine were compared between patient groups by considering the average z-score values retrieved per cell.

Cell-type and T cell clonotypic proportion comparisons

Significant differences in cell type abundances between the distinct clinical groups at the different timepoints were detected by using a binomial generalized linear model (GLM)[83]. A model taking into account Cluster and Condition was fitted, i.e., ~Cluster*Condition, by using Lme4 version 1.1-27.1. Emmeans version 1.6.2-1 was utilized to compare the odds ratios of different clinical groups for each

timepoint. The observed ratio (OR) is reported. *P*-values were adjusted with Benjamini–Hochberg (Supplementary Tables 1–6). To focus the comparative analysis of the response cohorts by single-cell transcriptomics on differences with clear biological relevance, we highlighted populations with both statistical significance and functional implications for immune modulation and effector cell function. Under this light, for differential abundance analyses, we applied a more stringent statistical threshold of $p < 0.01$ to avoid spurious findings. In addition, we have focused on comparing the cell subsets at baseline and 4 weeks post-CAR T infusion to eliminate the confounding factors of disease relapse and associated treatment in the early relapse cohort. Only patient groups from baseline and 4 weeks post-CAR T were included in the respective comparisons (Supplementary Fig. 1A). As a fixed number of cells were analyzed across the different timepoints, results are presented as relative abundance of each immune population to define the nature of the immune milieu and trajectory of change over time.

Trajectory interference and cell–cell communication analysis

Single-cell pseudotime trajectory was constructed in all cells using Slingshot v.2.0.0[84] based on the 20 dimensions of the Harmony embedding matrix. Cell-cell communication analysis was conducted separately among the major lineages and the distinct cell populations at the different timepoints using the CellChat v.1.0.0 R package[85]. A threshold of 20% in the average gene expression in each cell population was applied, while significant interactions and pathways were retained with a 0.05 *P* value cutoff.

Pathway analysis

A pathway score summarizes the expression of a set of functionally related genes[86]. Gene Ontology (GO) Biological Processes[87] was used to create a curated selection of pathways capturing the immune processes. Building on the methodology described in refs. 86,88, we used a rank-based approach to define the pathway scores, where the pathway score is the sum of the adjusted ranks of the genes in the pathway annotation scaled by the square root of the number of genes in the pathway. First, the ranks based on the UMI counts were calculated per gene for each cell, solving ties by selecting the minimum. Then, we scaled and centered the ranks across each cell. In order to account for the effect of rank sparsity for each gene, we split the scaled and centered ranks by their sign (positive or negative) and regressed out with a linear model the effect of the number of genes detected and the log of the total number of UMIs. Finally, we used the removeBatchEffect function from limma v.3.42.2 to adjust the pathway scores for batch effects.

scTCR sequencing, preprocessing, and data analysis

Cellranger v.4.0.0 V(D)J annotation pipeline[64] was utilized to retrieve clonotype information. Assembled contigs assigned to a raw clonotype ID were retained. Cell barcodes with TCR alpha chain and/or one TCR beta chain were retained. Each clonotype was characterized by the amino acid sequences of the CDR3 regions of the two chains across the distinct samples. Clonosize proportions were calculated by summarizing the number of each clonotype versus the total number of T cells with at least one clonotype. Public CDR3 β TCR clonotypes recognizing influenza, CMV, and EBV viral antigens were retrieved from VDJdb[89], IEDB[90], and McPAS[91] and compared against the CDR3 β TCR clonotypes of all the identified T cell populations. Fisher's exact test was applied to identify significantly enriched clonotypes per cell population at the post-CAR T timepoints compared to leukapheresis in the different cohorts. For each clonotype, we took into account its clonotypic frequency in the specific cell type relevant to the total number of T cells at leukapheresis and at the post-CAR T timepoint, versus the clonotypic frequency of all other α/β TCRs in the different timepoints. *P* values were adjusted using the Benjamini–Hochberg method. The significantly enriched clonotypes (FDR <0.05) with a clonotypic fold-change >1 at the post-CAR T timepoint versus leukapheresis were characterized as expanded, those with a clonotypic fold-change <1 as contracted, those with a clonotypic fold-change = 0 as novel, and the rest as persistent (FDR >0.05 and/or fold-change = 1).

T cell expansion model

The model incorporated five distinct characteristics: (i) the number of expanded α/β TCRs with TCR frequency >1 relative to the total T cells, and the number of expanded (TCR frequency >1) CD8, (ii) Tem/TGFβ1+ CXCR4+, (iii) Tem/highly cytotoxic, (iv) Tem/pro-inflammatory, and (v) CD4 CTL clonotypes relative to the total T cells. These relative abundances were combined in a naive Bayesian model, using the parameters usekernel = TRUE and adjust = 1 for Laplace smoothing. The distinct characteristics were scaled and centered accordingly. The model was trained and evaluated with leave-one-out cross-validation on 23 patients, 4 weeks post-CAR T (LtR, $n = 9$; R/NR, $n = 14$). Model deployment and evaluation were conducted using the caret v.6.0.94 package in R[92].

Data availability

The processed sequencing data generated in this study have been deposited in NCBI GEO under accession code GSE290722. Furthermore, raw sequencing data can be provided following a request for a Data Use Agreement with Kite Pharma, Inc., in accordance with participating patient consent. For additional information or to make a request, contact medinfo@kitepharma.com. All data generated or analyzed during this study are included in the Supplementary Information, the Source Data file, and are available on Zenodo https://doi.org/10.5281/zenodo.15007741)[93]. Source data are provided with this paper.

Code availability

Code for the analyses in this article is available on GitHub (https://github.com/ivlachos/ZUMA1_Single_Cell_DLBCL_Atlas, https://doi.org/10.5281/zenodo.15007741)[94].

References

1. Westin, J. R. et al. Efficacy and safety of CD19-directed CAR-T cell therapies in patients with relapsed/refractory aggressive B-cell lymphomas: observations from the JULIET, ZUMA-1, and TRANSCEND trials. *Am. J. Hematol.* **96**, 1295–1312 (2021).
2. Neelapu, S. S. et al. Axicabtagene ciloleucel CAR T-cell therapy in refractory large B-cell lymphoma. *N. Engl. J. Med.* **377**, 2531–2544 (2017).
3. Locke, F. L. et al. Long-term safety and activity of axicabtagene ciloleucel in refractory large B-cell lymphoma (ZUMA-1): a single-arm, multicentre, phase 1-2 trial. *Lancet Oncol.* **20**, 31–42 (2019).
4. Abramson, J. S. et al. Lisocabtagene maraleucel for patients with relapsed or refractory large B-cell lymphomas (TRANSCEND NHL 001): a multicentre seamless design study. *Lancet* **396**, 839–852 (2020).
5. Schuster, S. J. et al. Tisagenlecleucel in adult relapsed or refractory diffuse large B-cell lymphoma. *N. Engl. J. Med.* **380**, 45–56 (2019).
6. Garfall, A. L. et al. T-cell phenotypes associated with effective CAR T-cell therapy in postinduction vs relapsed multiple myeloma. *Blood Adv.* **3**, 2812–2815 (2019).
7. Fraietta, J. A. et al. Determinants of response and resistance to CD19 chimeric antigen receptor (CAR) T cell therapy of chronic lymphocytic leukemia. *Nat. Med.* **24**, 563–571 (2018).
8. Klaver, Y., van Steenbergen, S. C. L., Sleijfer, S., Debets, R. & Lamers, C. H. J. T cell maturation stage prior to and during GMP processing informs on CAR T cell expansion in patients. *Front. Immunol.* **7**, 648 (2016).

9. Xu, Y. et al. Closely related T-memory stem cells correlate with in vivo expansion of CAR.CD19-T cells and are preserved by IL-7 and IL-15. *Blood* **123**, 3750–3759 (2014).
10. Neelapu, S. S. et al. Five-year follow-up of ZUMA-1 supports the curative potential of axicabtagene ciloleucel in refractory large B-cell lymphoma. *Blood* **141**, 2307–2315 (2023).
11. Good, Z. et al. Post-infusion CAR TReg cells identify patients resistant to CD19-CAR therapy. *Nat. Med.* **28**, 1860–1871 (2022).
12. Haradhvala, N. J. et al. Distinct cellular dynamics associated with response to CAR-T therapy for refractory B cell lymphoma. *Nat. Med.* **28**, 1848–1859 (2022).
13. Bai, Z. et al. Single-cell antigen-specific landscape of CAR T infusion product identifies determinants of CD19-positive relapse in patients with ALL. *Sci. Adv.* **8**, eabj2820 (2022).
14. Melenhorst, J. J. et al. Decade-long leukaemia remissions with persistence of CD4 + CAR T cells. *Nature* **602**, 503–509 (2022).
15. Li, X. et al. Single-cell transcriptomic analysis reveals BCMA CAR-T cell dynamics in a patient with refractory primary plasma cell leukemia. *Mol. Ther.* **29**, 645–657 (2021).
16. Deng, Q. et al. Characteristics of anti-CD19 CAR T cell infusion products associated with efficacy and toxicity in patients with large B cell lymphomas. *Nat. Med.* **26**, 1878–1887 (2020).
17. Singh, N. et al. Impaired death receptor signaling in leukemia causes antigen-independent resistance by inducing CAR T-cell dysfunction. *Cancer Discov.* **10**, 552–567 (2020).
18. Sheih, A. et al. Clonal kinetics and single-cell transcriptional profiling of CAR-T cells in patients undergoing CD19 CAR-T immunotherapy. *Nat. Commun.* **11**, 219 (2020).
19. Finney, O. C. et al. CD19 CAR T cell product and disease attributes predict leukemia remission durability. *J. Clin. Invest.* **129**, 2123–2132 (2019).
20. Das, R. K., Vernau, L., Grupp, S. A. & Barrett, D. M. Naïve T-cell deficits at diagnosis and after chemotherapy impair cell therapy potential in pediatric cancers. *Cancer Discov.* **9**, 492–499 (2019).
21. Neelapu, S. S. et al. Outcomes of older patients in ZUMA-1, a pivotal study of axicabtagene ciloleucel in refractory large B-cell lymphoma. *Blood* **135**, 2106–2109 (2020).
22. Locke, F. L. et al. Tumor burden, inflammation, and product attributes determine outcomes of axicabtagene ciloleucel in large B-cell lymphoma. *Blood Adv.* **4**, 4898–4911 (2020).
23. Park, J. H. et al. Long-term follow-up of CD19 CAR therapy in acute lymphoblastic leukemia. *N. Engl. J. Med.* **378**, 449–459 (2018).
24. Lee, D. W. et al. T cells expressing CD19 chimeric antigen receptors for acute lymphoblastic leukaemia in children and young adults: a phase 1 dose-escalation trial. *Lancet* **385**, 517–528 (2015).
25. Locke, F. L. et al. Phase 1 results of ZUMA-1: a multicenter study of KTE-C19 anti-CD19 CAR T cell therapy in refractory aggressive lymphoma. *Mol. Ther.* **25**, 285–295 (2017).
26. Ali, S. A. et al. T cells expressing an anti-B-cell maturation antigen chimeric antigen receptor cause remissions of multiple myeloma. *Blood* **128**, 1688–1700 (2016).
27. Wang, X. et al. Phase 1 studies of central memory-derived CD19 CAR T-cell therapy following autologous HSCT in patients with B-cell NHL. *Blood* **127**, 2980–2990 (2016).
28. Davila, M. L. et al. Efficacy and toxicity management of 19-28z CAR T cell therapy in B cell acute lymphoblastic leukemia. *Sci. Transl. Med.* **6**, 224ra225 (2014).
29. Milone, M. C. & Bhoj, V. G. The pharmacology of T cell therapies. *Mol. Ther. Methods Clin. Dev.* **8**, 210–221 (2018).
30. Bhat, P., Leggatt, G., Waterhouse, N. & Frazer, I. H. Interferon-γ derived from cytotoxic lymphocytes directly enhances their motility and cytotoxicity. *Cell Death Dis.* **8**, e2836 (2017).
31. Gorelik, L. & Flavell, R. A. Immune-mediated eradication of tumors through the blockade of transforming growth factor-beta signaling in T cells. *Nat. Med.* **7**, 1118–1122 (2001).
32. Koizumi, S.-I. et al. JunB regulates homeostasis and suppressive functions of effector regulatory T cells. *Nat. Commun.* **9**, 5344 (2018).
33. Arcangeli, S. et al. CAR T cell manufacturing from naive/stem memory T lymphocytes enhances antitumor responses while curtailing cytokine release syndrome. *J. Clin. Invest.* **132**, e150807 (2022).
34. Singh, N., Perazzelli, J., Grupp, S. A. & Barrett, D. M. Early memory phenotypes drive T cell proliferation in patients with pediatric malignancies. *Sci. Transl. Med.* **8**, 320ra3 (2016).
35. Li, M. O., Wan, Y. Y., Sanjabi, S., Robertson, A.-K. L. & Flavell, R. A. Transforming growth factor-beta regulation of immune responses. *Annu. Rev. Immunol.* **24**, 99–146 (2006).
36. Li, M. O., Sanjabi, S. & Flavell, R. A. Transforming growth factor-beta controls development, homeostasis, and tolerance of T cells by regulatory T cell-dependent and -independent mechanisms. *Immunity* **25**, 455–471 (2006).
37. Jaiswal, H. et al. The NF-κB regulator Bcl-3 restricts terminal differentiation and promotes memory cell formation of CD8 + T cells during viral infection. *PLoS Pathog.* **17**, e1009249 (2021).
38. Chaix, J. et al. Cutting edge: CXCR4 is critical for CD8+ memory T cell homeostatic self-renewal but not rechallenge self-renewal. *J. Immunol.* **193**, 1013–1016 (2014).
39. Li, X.-Y. et al. NKG7 is required for optimal antitumor T-cell immunity. *Cancer Immunol. Res.* **10**, 154–161 (2022).
40. Gruber, T. et al. IL-32γ potentiates tumor immunity in melanoma. *JCI Insight* **5**, e138772 (2020).
41. Lucca, L. E. et al. Circulating clonally expanded T cells reflect functions of tumor-infiltrating T cells. *J. Exp. Med.* **218**, e20200921 (2021).
42. Li, H. et al. Dysfunctional CD8 T cells form a proliferative, dynamically regulated compartment within human melanoma. *Cell* **176**, 775–789.e18 (2019).
43. Mussbacher, M., Derler, M., Basílio, J. & Schmid, J. A. NF-κB in monocytes and macrophages - an inflammatory master regulator in multitalented immune cells. *Front. Immunol.* **14**, 1134661 (2023).
44. Schito, L. & Semenza, G. L. Hypoxia-inducible factors: master regulators of cancer progression. *Trends Cancer* **2**, 758–770 (2016).
45. Bai, R. & Cui, J. Mitochondrial immune regulation and anti-tumor immunotherapy strategies targeting mitochondria. *Cancer Lett.* **564**, 216223 (2023).
46. Yao, X. et al. SLC2A3 promotes macrophage infiltration by glycolysis reprogramming in gastric cancer. *Cancer Cell Int.* **20**, 503 (2020).
47. Li, X. et al. C5aR1 inhibition reprograms tumor associated macrophages and reverses PARP inhibitor resistance in breast cancer. *Nat. Commun.* **15**, 4485 (2024).
48. Eckfeld, C. et al. TIMP-1 is a novel ligand of amyloid precursor protein and triggers a proinflammatory phenotype in human monocytes. *J. Cell Biol.* **222**, e202206095 (2023).
49. Alaluf, E. et al. Heme oxygenase-1 orchestrates the immunosuppressive program of tumor-associated macrophages. *JCI Insight* **5**, e133929 (2020).
50. Jiang, G.-M. et al. The relationship between autophagy and the immune system and its applications for tumor immunotherapy. *Mol. Cancer* **18**, 17 (2019).
51. Cormican, S. & Griffin, M. D. Human monocyte subset distinctions and function: insights from gene expression analysis. *Front. Immunol.* **11**, 1070 (2020).
52. Le Gallou, S. et al. Nonclassical monocytes are prone to migrate into tumor in diffuse large B-cell lymphoma. *Front. Immunol.* **12**, 755623 (2021).
53. Hamilton, M. P. et al. CAR19 monitoring by peripheral blood immunophenotyping reveals histology-specific expansion and toxicity. *Blood Adv.* **8**, 3314–3326 (2024).

54. Thornton, A. M. & Shevach, E. M. CD4 + CD25+ immunoregulatory T cells suppress polyclonal T cell activation in vitro by inhibiting interleukin 2 production. *J. Exp. Med.* **188**, 287–296 (1998).
55. Takahashi, T. et al. Immunologic self-tolerance maintained by CD25 + CD4+ naturally anergic and suppressive T cells: induction of autoimmune disease by breaking their anergic/suppressive state. *Int. Immunol.* **10**, 1969–1980 (1998).
56. Hori, S., Nomura, T. & Sakaguchi, S. Control of regulatory T cell development by the transcription factor Foxp3. *Science* **299**, 1057–1061 (2003).
57. Fontenot, J. D., Gavin, M. A. & Rudensky, A. Y. Foxp3 programs the development and function of CD4 + CD25+ regulatory T cells. *Nat. Immunol.* **4**, 330–336 (2003).
58. Wu, T. D. et al. Peripheral T cell expansion predicts tumour infiltration and clinical response. *Nature* **579**, 274–278 (2020).
59. Scholler, N. et al. Tumor immune contexture is a determinant of anti-CD19 CAR T cell efficacy in large B cell lymphoma. *Nat. Med.* **28**, 1872–1882 (2022).
60. Kueberuwa, G., Kalaitsidou, M., Cheadle, E., Hawkins, R. E. & Gilham, D. E. CD19 CAR T cells expressing IL-12 eradicate lymphoma in fully lymphoreplete mice through induction of host immunity. *Mol. Ther. Oncolytics* **8**, 41–51 (2018).
61. Chmielewski, M., Kopecky, C., Hombach, A. A. & Abken, H. IL-12 release by engineered T cells expressing chimeric antigen receptors can effectively muster an antigen-independent macrophage response on tumor cells that have shut down tumor antigen expression. *Cancer Res.* **71**, 5697–5706 (2011).
62. Cheloni, G. et al. Synergism between CAR-T cells and a personalized tumor vaccine in hematological malignances. *Blood* **138**, 737–737 (2021).
63. Cheson, B. D. et al. Revised response criteria for malignant lymphoma. *J. Clin. Oncol.* **25**, 579–586 (2007).
64. Zheng, G. X. Y. et al. Massively parallel digital transcriptional profiling of single cells. *Nat. Commun.* **8**, 14049 (2017).
65. Lun, A. T. L. et al. EmptyDrops: distinguishing cells from empty droplets in droplet-based single-cell RNA sequencing data. *Genome Biol.* **20**, 63 (2019).
66. Griffiths, J. A., Richard, A. C., Bach, K., Lun, A. T. L. & Marioni, J. C. Detection and removal of barcode swapping in single-cell RNA-seq data. *Nat. Commun.* **9**, 2667 (2018).
67. Stuart, T. et al. Comprehensive integration of single-cell data. *Cell* **177**, 1888–1902.e21 (2019).
68. Korsunsky, I. et al. Fast, sensitive and accurate integration of single-cell data with Harmony. *Nat. Methods* **16**, 1289–1296 (2019).
69. Freytag, S. Schex. *Bioconductor* https://doi.org/10.18129/B9.BIOC.SCHEX (2019).
70. Aran, D. et al. Reference-based analysis of lung single-cell sequencing reveals a transitional profibrotic macrophage. *Nat. Immunol.* **20**, 163–172 (2019).
71. Domínguez Conde, C. et al. Cross-tissue immune cell analysis reveals tissue-specific features in humans. *Science* **376**, eabl5197 (2022).
72. Wolock, S. L., Lopez, R. & Klein, A. M. Scrublet: computational identification of cell doublets in single-cell transcriptomic data. *Cell Syst.* **8**, 281–291.e9 (2019).
73. Li, B. et al. Cumulus provides cloud-based data analysis for large-scale single-cell and single-nucleus RNA-seq. *Nat. Methods* **17**, 793–798 (2020).
74. Delorey, T. M. et al. COVID-19 tissue atlases reveal SARS-CoV-2 pathology and cellular targets. *Nature* **595**, 107–113 (2021).
75. McGinnis, C. S., Murrow, L. M. & Gartner, Z. J. DoubletFinder: doublet detection in single-cell RNA sequencing sata using artificial nearest neighbors. *Cell Syst.* **8**, 329–337.e4 (2019).
76. Law, C. W., Chen, Y., Shi, W. & Smyth, G. K. voom: precision weights unlock linear model analysis tools for RNA-seq read counts. *Genome Biol.* **15**, R29 (2014).
77. Soneson, C. & Robinson, M. D. Bias, robustness and scalability in single-cell differential expression analysis. *Nat. Methods* **15**, 255–261 (2018).
78. Robinson, M. D. & Oshlack, A. A scaling normalization method for differential expression analysis of RNA-seq data. *Genome Biol.* **11**, R25 (2010).
79. Robinson, M. D., McCarthy, D. J. & Smyth, G. K. edgeR: a Bioconductor package for differential expression analysis of digital gene expression data. *Bioinformatics* **26**, 139–140 (2010).
80. Phipson, B., Lee, S., Majewski, I. J., Alexander, W. S. & Smyth, G. K. Robust hyperparameter estimation protects against hypervariable genes and improves power to detect differential expression. *Ann. Appl. Stat.* **10**, 946–963 (2016).
81. Andreatta, M. & Carmona, S. J. UCell: robust and scalable single-cell gene signature scoring. *Comput. Struct. Biotechnol. J.* **19**, 3796–3798 (2021).
82. Jiang, P. et al. Systematic investigation of cytokine signaling activity at the tissue and single-cell levels. *Nat. Methods* **18**, 1181–1191 (2021).
83. Pita-Juarez, Y. et al. A single-nucleus and spatial transcriptomic atlas of the COVID-19 liver reveals topological, functional, and regenerative organ disruption in patients. *Genome Biol.* **26**, 56 (2025).
84. Street, K. et al. Slingshot: cell lineage and pseudotime inference for single-cell transcriptomics. *BMC Genomics* **19**, 477 (2018).
85. Jin, S. et al. Inference and analysis of cell-cell communication using CellChat. *Nat. Commun.* **12**, 1088 (2021).
86. Pita-Juárez, Y. et al. The pathway coexpression network: revealing pathway relationships. *PLoS Comput. Biol.* **14**, e1006042 (2018).
87. The Gene Ontology Consortium. The Gene Ontology Resource: 20 years and still GOing strong. *Nucleic Acids Res.* **47**, D330–D338 (2019).
88. Altschuler, G. M. et al. Pathprinting: an integrative approach to understand the functional basis of disease. *Genome Med.* **5**, 68 (2013).
89. Bagaev, D. V. et al. VDJdb in 2019: database extension, new analysis infrastructure and a T-cell receptor motif compendium. *Nucleic Acids Res.* **48**, D1057–D1062 (2020).
90. Vita, R. et al. The immune epitope database (IEDB): 2018 update. *Nucleic Acids Res.* **47**, D339–D343 (2019).
91. Tickotsky, N., Sagiv, T., Prilusky, J., Shifrut, E. & Friedman, N. McPAS-TCR: a manually curated catalogue of pathology-associated T cell receptor sequences. *Bioinformatics* **33**, 2924–2929 (2017).
92. Kuhn, M. Building predictive models in R using the caret package. *J. Stat. Softw.* **28**, 1–26 (2008).
93. Dimitra, K., Yered, P.-J. & Ioannis, V. Durable response to CAR T is associated with elevated activation and clonotypic expansion of the cytotoxic native T cell repertoire. *Zenodo* (2025).
94. ivlachos/ZUMA1_Single_Cell_DLBCL_Atlas. *GitHub* https://github.com/ivlachos/ZUMA1_Single_Cell_DLBCL_Atlas (2025).

Acknowledgements

The authors thank Dina Stroopinsky and all members of the Vlachos lab for critical discussion. This research was funded by Kite, a Gilead company, Santa Monica, CA, USA. D.K. acknowledges support from the George and Marie Vergottis Foundation. Data analyses have been performed using computational resources from the BIDMC Spatial Technologies Unit (RRID:SCR_024905).

Author contributions

G.C., D.K., I.S.V. and D.A. designed the study. G.C. and D.K. contributed equally as co-first authors. G.C., D.T. and I.S. carried out experiments. D.K., Y.P.-J. and E.K. performed computational analysis. G.C., D.K. and Z.A. worked on the deep cell type characterization. G.C., D.K., I.S.V. and

D.A. wrote the manuscript with input from Y.P.-J., D.T., E.K., J.L., Z.A., I.S., G.C., K.R., B.M., G.T., J.K., M.M. and J.R. All authors reviewed and approved the final version of the manuscript.

Competing interests

B.Miles, G. Tiwari, J. Kim, and M. Mattie report employment with Kite, a Gilead company, and stock or other ownership in Gilead Sciences. J. Rosenblatt reports consulting with Attivare, Parexel, Clario/Bioclinica, Imaging Endpoint, and Wolters Kluwer Health, Inc. Serves on a DSMB with Karyopharm. Grants and nonfinancial support from Celgene, BMS, and Sanofi outside the submitted work. I.S. Vlachos consults for Guidepoint Global, Chronicle Medical Software Inc., and Mosaic outside of the submitted work. D. Avigan reports grants from MMRF, CTN (NIHLBI), Celgene, Pharmacyclics, AbbVie, and Kite Pharma. Other support from Juno, Partners TX, Karyopharm, BMS, Takeda, Legend Bio Tech, Chugai, Janssen, Parexel, Sanofi, Regeneron, and Arcellix outside the submitted work. D. Avigan and J. Rosenblatt hold a patent, US patent 11, 026,921 entitled, "Compositions and Methods of Treating Cancer". No disclosures were reported by the other authors. This research was funded by Kite, a Gilead company, Santa Monica, CA, USA.

Additional information

Supplementary information The online version contains supplementary material available at https://doi.org/10.1038/s41467-025-59904-x.

Correspondence and requests for materials should be addressed to David Avigan.

Peer review information *Nature Communications* thanks Stephen Gottschalk, Michael Jain and Andrew P Jallouk for their contribution to the peer review of this work. A peer review file is available.